Journal of Power Sources 225 (2013) 304–310

Contents lists available at SciVerse ScienceDirect

Journal of Power Sources

journal homepage: www.elsevier.com/locate/jpowsour

Short communication

Ultrahigh capacitance of nanoporous metal enhanced conductive polymer pseudocapacitors

Ying Hou [a], Luyang Chen [a], Ling Zhang [a], Jianli Kang [a], Takeshi Fujita [a], Jianhua Jiang [b], Mingwei Chen [a,b,c,*]

[a] WPI-Advanced Institute for Materials Research, Tohoku University, Sendai 980-8577, Japan
[b] State Key Laboratory of Metal Matrix Composites, and School of Materials Science and Engineering, Shanghai Jiao Tong University, Shanghai 200030, China
[c] JST, CREST, 4-1-8 Honcho Kawaguchi, Saitama 332-0012, Japan

HIGHLIGHTS

- NPG-PPy hybrid electrodes are fabricated by combining dealloying and electropolymerization.
- Nanoporous hybrid structure facilitates charge transport and thus has low internal resistance.
- Ultrahigh energy densities of ~100 Wh kg^{-1} in a 3-electrode configuration, comparable to NiMH batteries, can be achieved.
- High power density of ~57 kW kg^{-1} is retained along with ultrahigh capacitance.
- The hybrid electrodes keep up to 85% the maximum capacitance after 3000 cycles.

ARTICLE INFO

Article history:
Received 28 June 2012
Received in revised form
15 October 2012
Accepted 19 October 2012
Available online 29 October 2012

Keywords:
Nanoporous metal
Polypyrrole
Supercapacitor
Energy storage

ABSTRACT

A high energy density is critical for supercapacitors to supersede conventional batteries for the applications where both high power and high energy are demanded. Here we report nanoporous metal/conductive polymer hybrid electrodes fabricated by electrochemically plating conductive polypyrrole into nanoporous channels of a dealloyed nanoporous metal. The low electric resistance and open porosity of the nanoporous metal give rise to excellent conductivity of electrons and ions and hence dramatically improved electrochemical performances of the pseudocapacitive polypyrrole. Supercapacitors based on the hybrid electrodes show an ultrahigh energy density of ~100 Wh kg^{-1} in a three-electrode, comparable to NiMH batteries, as well as high power density of ~57 kW kg^{-1}. Cycling stability measurements demonstrate that the hybrid electrode can retain 85% of the maximum capacitance after 3000 cycles and the degeneration is mainly caused by the dissolution of polypyrrole during charge/discharge cycling.

1. Introduction

With the rapid development of the economy and the exhaustion of fossil fuels, electrochemical energy storage and conversion systems, such as batteries, fuel cells and supercapacitors, with both high power density and energy density are highly demanded as alternative energy sources of electric and hybrid electric vehicles in green energy innovation. [1–5] Among these energy devices, supercapacitors are expected to bridge the gap between conventional capacitors with high power density but low energy density and batteries that have high energy density but low power density [6–11] because there is still a large space for supercapacitors to further improve their energy density with retaining high power density. There are two mechanisms for the charge storage of supercapacitors. One is so called electrochemical double-layer capacitance by non-Faradic surface ion adsorption; [6,7,12,13] and the other is the pseudocapacitance by fast Faradic redox reactions at electrode/electrolyte interfaces [14–16] These two mechanisms can work separately or together, depending on the electrode materials used in supercapacitors [4,17,18] Conductive porous materials with large surface areas, such as active carbon and nanoporous metals, [1,9,10,19,20] are desired electrodes for electrochemical double-layer supercapacitors. In general, electrochemical double-layer supercapacitors have obvious advantages in power density and lifetimes, but their energy density is still much lower than that of batteries [2,9,18,21] Therefore, it has been the recent topic of intense research to search for new electrode materials that can provide high energy density, comparable to batteries. It has been known that transition

* Corresponding author. WPI-Advanced Institute for Materials Research, Tohoku University, Sendai 980-8577, Japan. Tel.: +81 22 217 5959; fax: +81 22 215 5994.
E-mail address: mwchen@wpi-aimr.tohoku.ac.jp (M. Chen).

0378-7753/$ – see front matter © 2012 Elsevier B.V. All rights reserved.
http://dx.doi.org/10.1016/j.jpowsour.2012.10.067

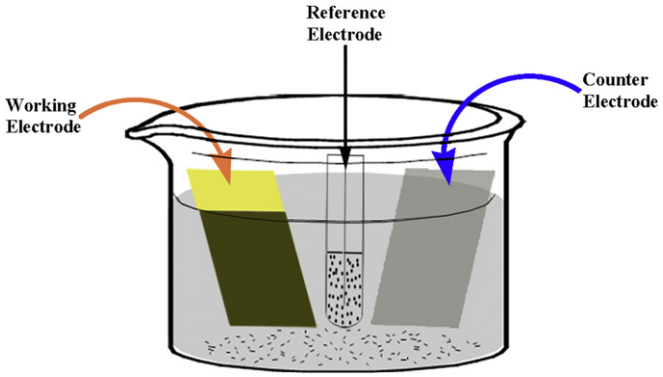

Fig. 1. Schematic illustration of the three-electrode system for capacitance measurements in this study.

metal oxides, such as MnO_2 and RuO_2, and conductive polymers, such as polyaniline (PANI) and polypyrrole (PPy), have high theoretical capacitance values for pseudocapacitors [3,22–25] However, their capacitive performances are limited by high electric resistance and low cycling stability. Particularly, the attainable energy density is often an order of magnitude lower than their theoretical assessment. Recently, by utilizing the excellent conductivity, large internal surfaces and open porosity of nanoporous gold (NPG), Lang et al. successfully incorporated pseudocapacitive MnO_2 and PANI into NPG and fabricated novel hybrid electrodes for supercapacitors with a high energy density [26,27]. Meng and Ding also documented the fabrication of an ultrathin, flexible, all-solid-state supercapacitor based on PPy-decorated NPG [28] In this study, we developed a PPy/NPG hybrid electrode that offers an ultrahigh energy density of ~100 Wh kg^{-1} in a three-electrode mode, comparable to NiMH batteries, and retained high power density of ~57 kW kg^{-1} as well as good cycling stability.

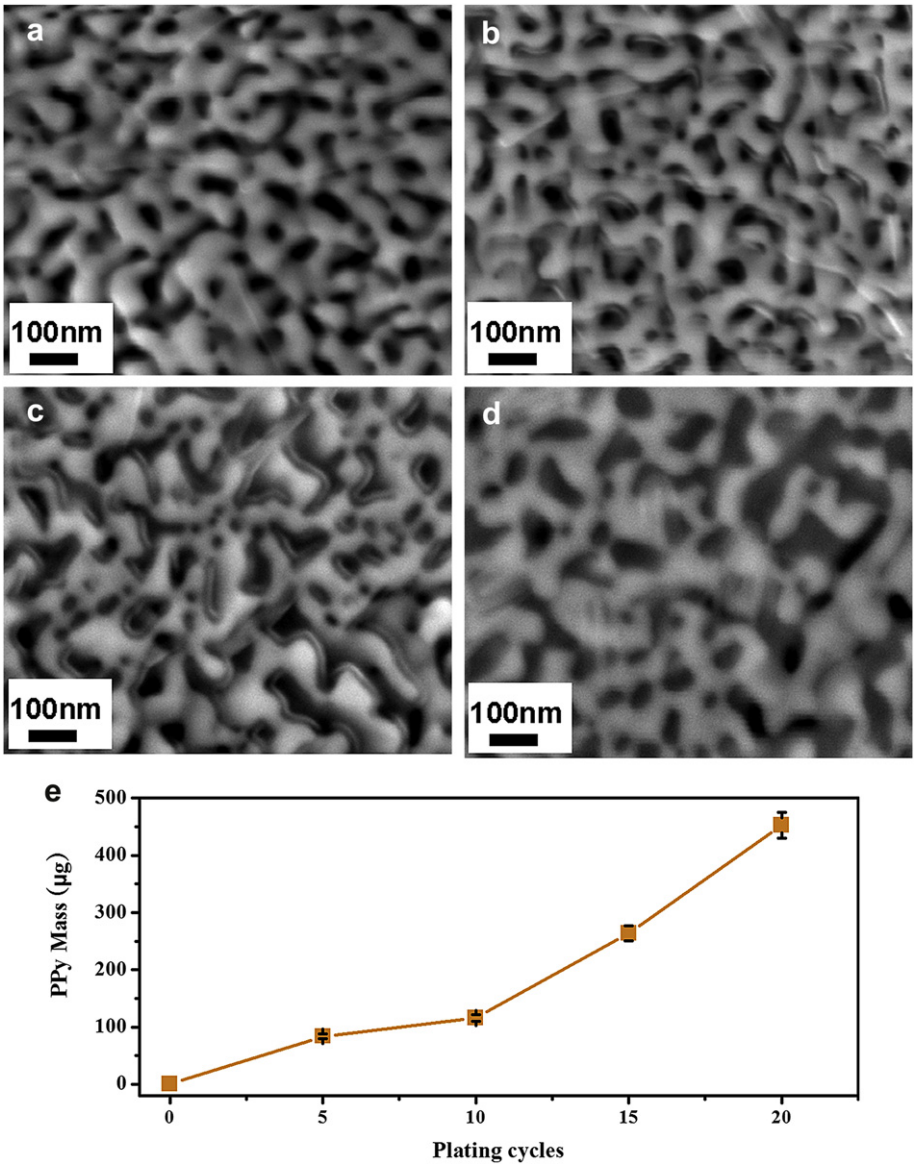

Fig. 2. . SEM images of PPy/NPG composites with different plating cycles: (a) 5 cycles; (b) 10 cycles; (c) 15 cycles; and (d) 20 cycles. (e) The relationship between plating cycles and PPy loading amounts.

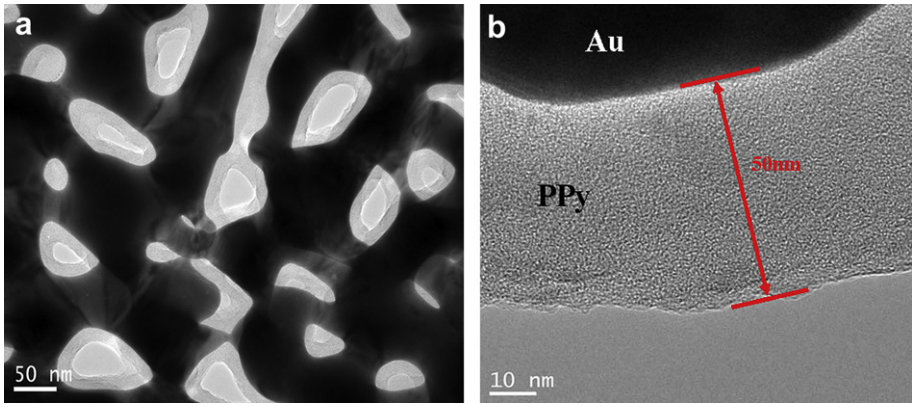

Fig. 3. . Microstructure of PPy/NPG composite with 15 cycle PPy loading. (a) Bright-field TEM micrograph showing a nanoporous core–shell structure. (b) HRTEM image of the interfacial structure of PPy/NPG, revealing that the amorphous PPy bonds well with the metal ligaments.

2. Experimental

2.1. Fabrication of nanoporous gold (NPG)

We fabricated NPG by chemically dealloying $Ag_{65}Au_{35}$ (at. %) films. Since the formation of a gold oxide layer on the ligaments during electrochemical dealloying may significantly affect the double-layer capacitive performance [33], in this study the dealloying was performed by free corrosion in a 69% HNO_3 solution for 8 h at room temperature. The nanoporous structure was quenched by pure water (18.2 MΩ cm), and the residual acid within the nanoporous channels was thoroughly removed by rinsing with water [34,35].

2.2. Fabrication of PPy/NPG composite and assembly of a supercapacitor device based on PPy/NPG electrodes

PPy/NPG hybrid electrodes were fabricated by an electrochemical plating method. 1.38 mL Pyrrole (99.0% Wako Pure Chemical Industries, Ltd.) and 5.77 g sodium dodecyl sulfonate

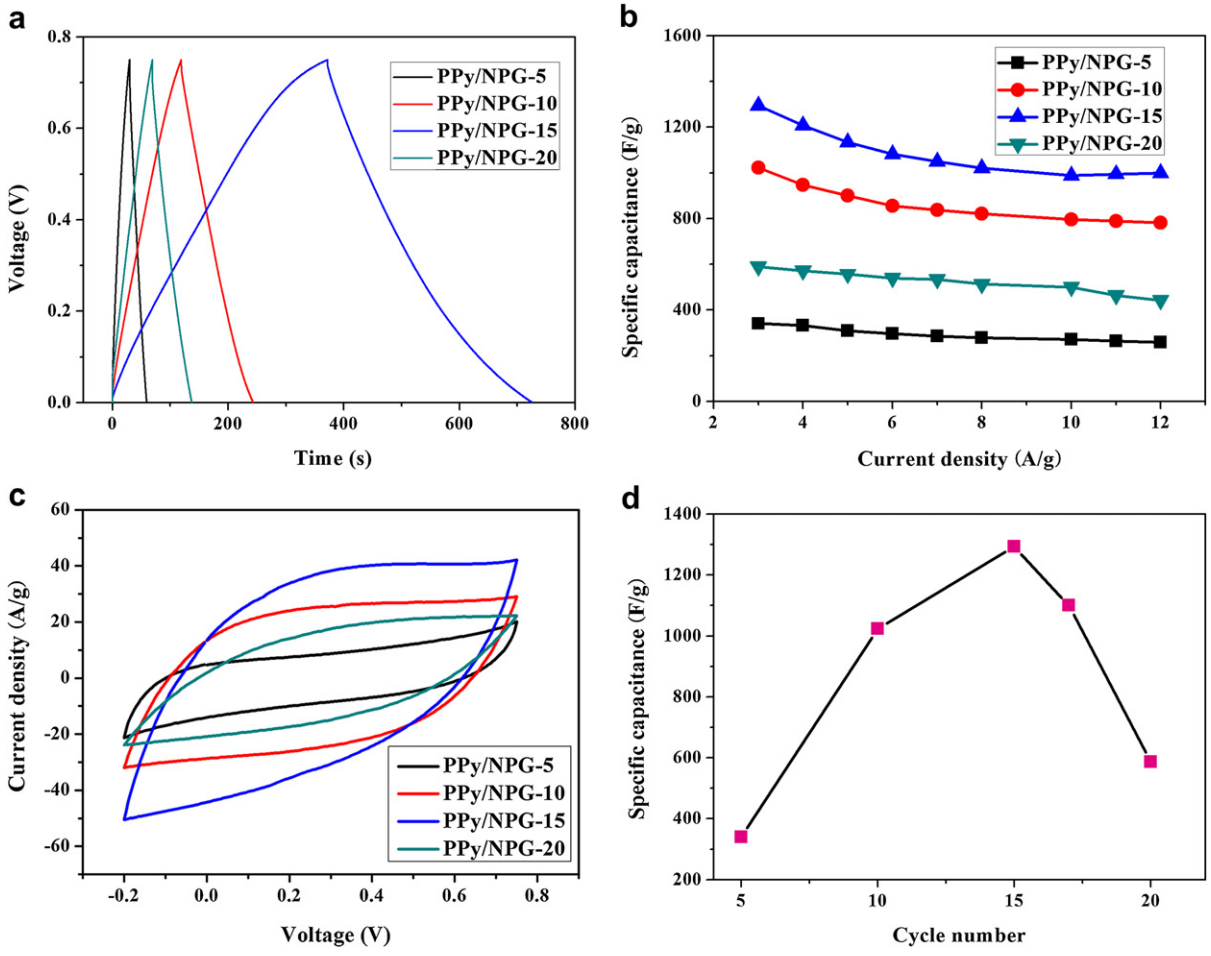

Fig. 4. Capacitive performances of the PPy/NPG hybrid electrodes. (a) Galvanostatic charge/discharge curves at 6 A g^{-1} with different PPy loading amounts. (b) Specific capacitance obtained at different current densities. (c) CV curves at a scan rate of 80 mV/. (d) Specific capacitance as a function of the cycle number of electrochemical polymerization.

(SDS, Kanto Chemical Co., Inc.) were dissolved in 200 mL distilled water to form a 0.1 M solution. A NPG film was attached on a polyethylene terephthalate (PET) membrane that was used as a holder for the electrochemical plating. Half of the NPG film was covered by a cotton paper while the remaining half was functioned as the conductive area. The anodic oxidation synthesis of pyrrole on NPG was conducted by cyclic voltammetry (CV) with a potential window ranging from −0.2 V to 0.9 V. The synthesis was performed in a standard three-electrode system with a platinum sheet as the counter electrode, Ag/AgCl as the reference electrode, and an NPG film on a PET membrane as the working electrode. The loading amount of PPy was controlled by the cycling number of plating.

2.3. Microstructure characterization

The microstructure and chemical composition of the samples were characterized by a field-emission scanning electron microscope (SEM, JEOL JIB-4600F, 15 keV) and a field-emission transmission electron microscope (TEM, JEOL JEM-2100F, 200 keV). Raman spectra were recorded using a Renishaw Raman microscope with excitation at 632.8 nm using a He–Ne laser at a beam size of ~1 μm.

2.4. Electrochemical measurements of PPy/NPG supercapacitors

The electrochemical properties and capacitances of the PPy/NPG composites were studied in a three-electrode system by CV and galvanostatic charge/discharge using an Iviumstat electrochemical analyzer. The system was constructed using a platinum sheet as the counter electrode, Ag/AgCl as the reference electrode, and the PPy/NPG composites as the working electrode. A 1 M $HClO_4$ aqueous solution was used as the electrolyte for the standard PPy/NPG based supercapacitors.

3. Results and discussion

3.1. Microstructure of PPy/NPG hybrid electrodes

We use an electrochemical plating method to fabricate PPy/NPG hybrid electrodes. The configuration of the three-electrode system is shown in the schematic diagram of Fig. 1. The loading amount and the layer thickness of PPy can be well controlled by the cycle number of the electrochemical plating. As shown in Fig. 2a–d, the loading amount of PPy gradually increases with the cycling number from 5 to 20 times. Quantitative measurements indicate the nearly linear dependence of the PPy amount with the plating cycles. The SEM images illustrate an open nanopore structure with an average size of gold ligaments and nanopore channels of ~80 nm [29] The PPy coating forms a core–shell structure in which the conducting polymer uniformly covers the internal surfaces of the metal ligaments as shown in the SEM and bright-field TEM images (Figs. Fig. 2c and 3a). The PPy layers display bright contrast as the shell while the gold skeleton shows dark contrast. High-resolution TEM (HRTEM) reveals the well-bonded PPy/Au interface and the

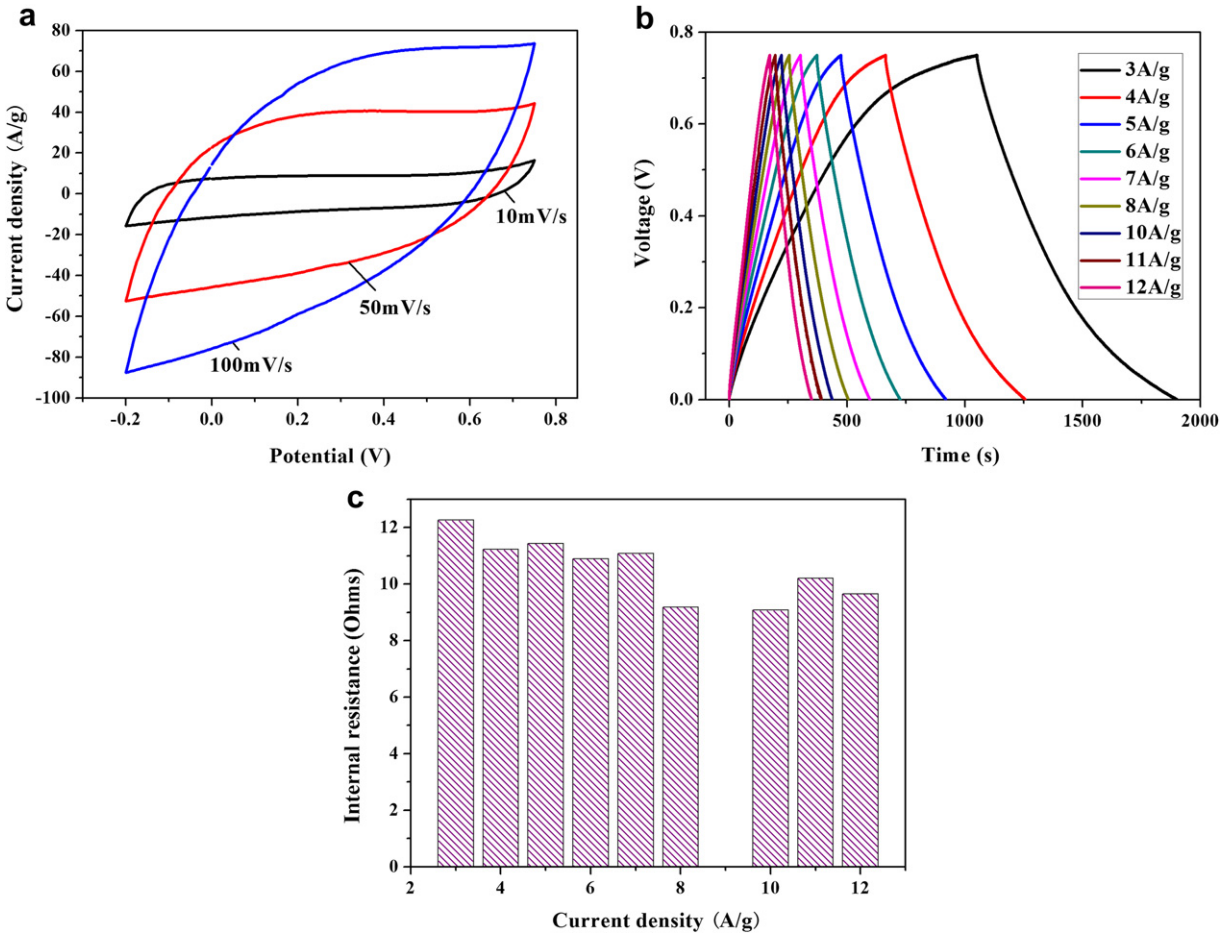

Fig. 5. Electrochemical performances of the PPy/NPG hybrid electrode with the PPy coating loaded by 15-cycle electrochemical polymerization. (a) Cyclic voltammograms at different scan rates in 1 M $HClO_4$. (b) Galvanostatic charge/discharge curves at different current densities. (c) Internal resistance of the NPG-based hybrid electrode in 1 M $HClO_4$ measured at the discharge current densities of 3, 4, 5, 6, 7, 8, 10, 11, and 12 A g^{-1}.

amorphous structure of the deposited PPy without any well-defined periodic lattice (Fig. 3b). The core–shell structure with open porosity promises the good conductivity of the PPy/NPG composite and the effective rapid ion transport between the electrolyte and the composite.

3.2. Capacitive performance of PPy/NPG hybrid electrodes

Representative galvanostatic charge/discharge curves of the PPy/NPG supercapacitors as the function of the PPy plating cycles (equal to the PPy loading amount) at a current density of 6 A g^{-1} are illustrated in Fig. 4a. The discharge time of the supercapacitors dramatically increases with the plating cycles and the 15-cycle composite shows the longest discharge time. Fig. 4b displays the volumetric capacitances (C_s) of the PPy/NPG electrodes with different plating cycles as the function of the applied current density. The capacitance increases with the plating cycles from 3 to 15 cycles and reaches the maximum value at 15 plating cycles. The ultrahigh specific capacitance C_s is of ~1300 F g^{-1} at the current density of 3 A g^{-1} and retains to be ~1000 F g^{-1} at the high current density of ~12 A g^{-1} (Fig. 4b). Here, C_s was calculated according to the charge/discharge curves, $C_s = i/[-(\Delta E/\Delta t)m]$, with i being the applied current; $-\Delta E/\Delta t$, the slope of the discharge curve after the voltage drop at the beginning of each discharge (ΔE_{IR}); and m, the mass of composite electrodes. Fig. 4c illustrates cyclic voltammograms of the PPy/NPG electrodes as a function of plating cycles at a scan rate of 80 mV s^{-1}. It is consistent with the charge/discharge measurements that more plating cycles give rise to a larger CV area and hence higher capacitance (Fig. 4c). As shown in Fig. 4d, the specific capacitance of the hybrid electrodes with different amount of PPy dramatically increases from 5 to 15 plating cycles whereas further increasing the PPy loading leads to the obvious decrease of the volumetric capacitance because the excess PPy creates channel congestion and prevents effective contact between the core–shell PPy/NPG and the electrolyte.

The electrochemical performances of the best PPy/NPG electrode with 15-cycle PPy plating were systematically characterized by the three-electrode system in a 1 M $HClO_4$ aqueous solution at room temperature. The CV curves of the PPy/NPG electrode were measured at the scan rates from 10 mV s^{-1} to 100 mV s^{-1}. As shown in Fig. 5a, the curves show a symmetrical and near rectangular shape, indicating good capacitive performance over the potential window of −0.2 V to 0.75 V. Fig. 5b displays the representative galvanostatic charge/discharge curves of the PPy/NPG electrode obtained at different current densities. The discharge curves show two stages. One is caused by both the fast Faradic redox reaction and non-Faradic surface ion adsorption of the PPy/NPG composite with a long voltage duration from 0 V to 0.7 V. The double-layer capacitive behavior of the nanoporous structure results in the other voltage stage with short discharge duration from 0.7 V to 0.75 V [30]. The internal resistance of the PPy/NPG electrode was calculated by using the equation $R = \Delta E_{IR}/2i$. The very low internal resistance at all tested current densities (Fig. 5c) further proves the occurrence of fast electron transport in the hybrid electrode, which is associated with the highly conductive gold network and excellent contact between PPy and metal ligaments. The Ragone plot of the PPy/NPG supercapacitor, compared with other PPy based devices, is shown in Fig. 6a. The specific power density P and energy density E were calculated using the equations: $P = V^2/(4Rm)$ and $E = 0.5CV^2$, respectively. Here, V is the cutoff voltage, C is the measured device capacitance, and R is the internal resistance of the device (Table 1). The ultrahigh energy density of up to ~100 Wh kg^{-1} along with the power density of up to 57 kW kg^{-1} of the PPy/NPG based supercapacitor are approximately 10 times and 2 times higher than a PPy-RGO based supercapacitor, respectively [31]. Although the

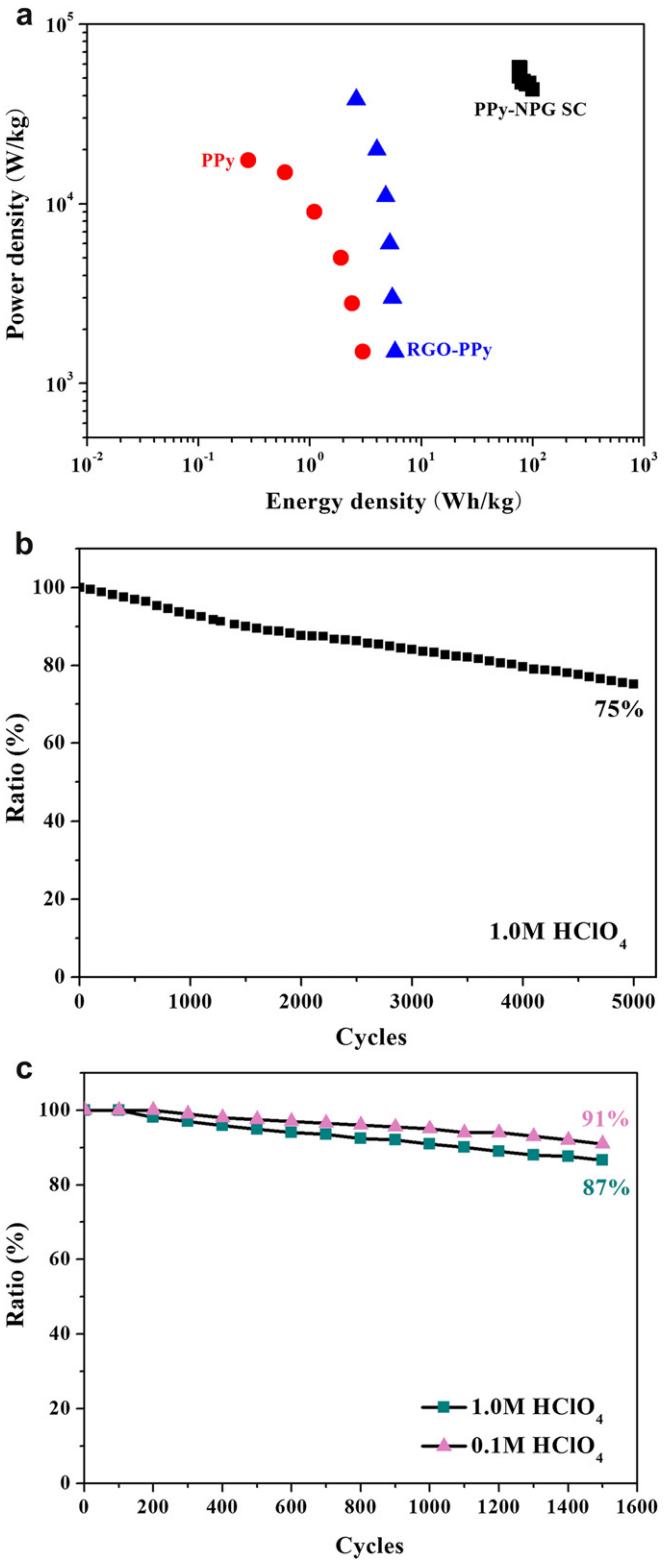

Fig. 6. (a) Ragone plot of the NPG-based PPy pseudocapacitors along with the reported PPy-based supercapacitors for comparsion. (b) Capacitance retention ratio of the PPy/NPG electrode from the 1st to the 5000th cycle at a scan rate of 100 mV s^{-1} in 1 M $HClO_4$ acid solutions. (b) Capacitance retention ratio of the PPy/NPG electrode from the 1st to the 1500th cycle at a scan rate of 100 mV s^{-1} in 1 M (green line) and 0.1 M $HClO_4$ (pink line) acid solutions. (For interpretation of the references to color in this figure legend, the reader is referred to the web version of this article.)

Table 1
Internal resistance, power densities and energy densities of NPG-based PPy pseudocapacitors with different PPy plating cycles.

Current density ($A\ g^{-1}$)	Parameters											
	R (Ohms)				P ($kW\ kg^{-1}$)				E ($Wh\ kg^{-1}$)			
	Samples (plating cycles)											
	5	10	15	20	5	10	15	20	5	10	15	20
3	16.67	14.30	12.26	15.48	1.05×10^4	3.56×10^4	4.31×10^4	2.69×10^4	32.60	80.48	100.20	67.64
4	17.46	15.00	11.22	16.54	1.23×10^4	3.60×10^4	4.60×10^4	2.78×10^4	26.43	76.59	93.32	65.42
5	17.98	15.32	11.44	16.30	1.30×10^4	3.65×10^4	4.70×10^4	2.87×10^4	25.66	74.67	87.38	64.78
6	18.07	15.20	10.90	15.42	1.44×10^4	3.74×10^4	4.72×10^4	2.92×10^4	23.80	73.45	83.17	64.07
7	18.00	14.01	11.08	15.34	1.69×10^4	3.80×10^4	4.82×10^4	2.96×10^4	22.69	71.97	80.44	60.53
8	18.10	14.35	9.18	14.98	1.71×10^4	3.93×10^4	5.09×10^4	2.99×10^4	21.87	71.60	78.25	59.27
10	17.98	13.82	9.70	16.23	1.83×10^4	4.05×10^4	5.38×10^4	3.07×10^4	21.17	70.59	75.96	57.41
11	18.02	13.49	10.21	15.8	1.85×10^4	4.11×10^4	5.71×10^4	3.11×10^4	20.63	69.64	75.67	56.00
12	18.05	14.56	9.65	16.12	1.91×10^4	4.16×10^4	5.76×10^4	3.15×10^4	20.07	68.00	75.66	50.25

high energy density measured from three-electrode cell is higher than that in a two-electrode configuration, the energy density at high power of the PPy/NPG composite in the three-electrode mode is comparable to that of the NiMH batteries, which sheds light on the supercapacitor devices for high energy applications. The ultrahigh capacitance of the PPy/NPG composite also makes the novel conductive polymer and nanoporous metal based supercapacitors a promising candidate for the high power and high energy applications.

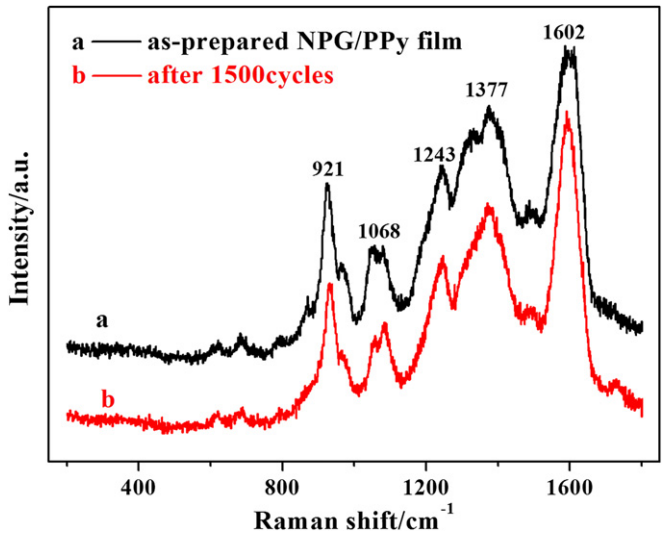

Fig. 7. Raman spectra of the PPy/NPG electrode before the electrochemical cycling (line a) and after 1500 cycles (line b).

3.3. Cycling stability of PPy/NPG hybrid electrodes

Conductive polymer based supercapacitors usually suffer from low cycling stability. For the PPy/NPG based supercapacitor, the cycling stability was measured by CV testing at a scan rate of 100 mV s^{-1}. The results reveal that the PPy/NPG electrode possesses much better stability compared to other PPy based supercapacitors. The high capacitance can keep up to 85% after 3000 cycles (Fig. 6b). Even after 5000 cycles, the capacitance still retain to be 75% of the maximum capacitance. Raman spectroscopy and TEM were employed to investigate the structure changes caused by electrochemical cycling. Fig. 7 shows the Raman spectra of the PPy loaded into the nanopore channels of NPG. The characteristic bands of PPy at 1602 cm^{-1}, 1377 cm^{-1}, 1068 cm^{-1}, etc. can be identified in the as-prepared sample. The 1602 cm^{-1} band has been assigned to an overlap of bands arising from the radical cation and dication and the 1068 cm^{-1} band is from the CH in-plane bending vibration [32] After 1500 cycles, obvious structure change of PPy cannot be found from the Raman spectra, implying that the degeneration of the capacitance is not associated with the irreversible PPy structure transition. Fig. 8a and b show the TEM micrographs of the PPy/NPG composite after 1500 cycles. The post-mortem inspection suggests that the PPy coatings still bond well with the NPG substrate after 1500 cycles but the PPy layer becomes evidently thinner, compared to that in the as-prepared one (Fig. 3a and b). Therefore, the degeneration of the PPy/NPG electrode is mainly caused by the dissolution of PPy during charge/discharge cycling in the 1 M $HClO_4$

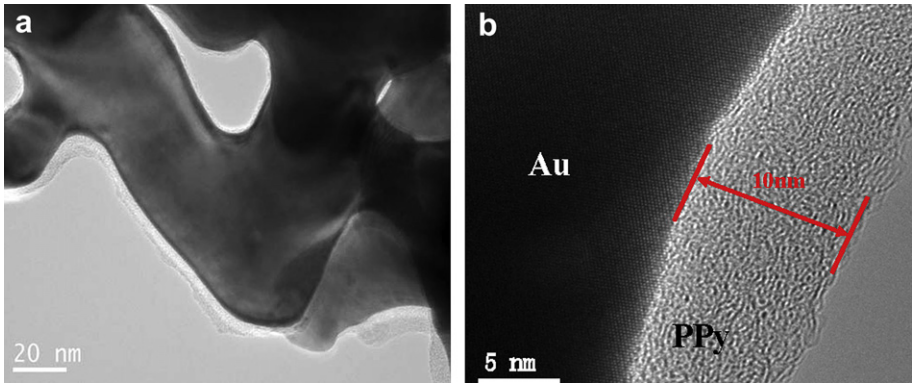

Fig. 8. Microstructure characterization of the 1500 cycled PPy/NPG electrode. (a) Bright-field TEM micrograph; and (b) HRTEM image. The NPG substrate does not show obvious change after 1500 cycles whereas the PPy coating becomes much thinner than that of the as-prepared hybrid electrode.

aqueous electrolyte. In order to confirm this result, a diluted electrolyte of 0.1 M $HClO_4$ aqueous solution was used for the cycling stability experiment at a scan rate of 100 mV s^{-1}. Fig. 6c (pink line). Compare to 1 M $HClO_4$ aqueous electrolyte (Fig. 6c (green line)), the capacitance can keep up to 91% after 1500 cycles. Thus, the cycling stability of the PPy/NPG electrode is expected to be further improved by optimizing the electrolyte that can effectively prevent the dissolution of PPy.

4. Conclusion

In summary, we have developed a core–shell NPG-PPy hybrid electrode by the combination of dealloying and electropolymerization. The nanoporous structure of the electrode can effectively facilitate fast ion transport between the conductive polymer and the electrolyte through open nanopore channels. The NPG substrate provides high electric conductivity and simultaneously serves as the electron collectors. The novel supercapacitor based on the PPy/NPG hybrid electrode exhibits ultrahigh capacitance and improved power and energy densities as one of the best PPy based pseudocapacitive devices known so far.

Acknowledgments

This research was sponsored JST-CREST 'Phase Interface Science for Highly Efficient Energy Utilization', JST; Global COE for Materials Research and Education; and World Premier International (WPI) Research Center Initiative for Atoms, Molecules and Materials, MEXT, Japan. T.F is supported by PRESTO, JST, Japan.

References

[1] B.E. Conway, Electrochemical Supercapacitor, Scientific Fundamentals and Technological Applications, Kluwer Academic/Plenum Press, New York, 1999.
[2] M. Winter, R.J. Brodd, Chem. Rev. 104 (2004) 4245–4270.
[3] R. Liu, S.B. Lee, J. Am. Chem. Soc. 130 (2008) 2942–2943.
[4] C. Liu, F. Li, L.-P. Ma, H.-M. Cheng, Adv. Mater. 22 (2010) E28–E62.
[5] A.S. Arico, P. Bruce, B. Scrosati, J.-M. Tarascon, W. van Schalkwijk, Nat. Mater. 4 (2005) 366–377.
[6] R. Kötz, M. Carlen, Electrochim. Acta 45 (2000) 2483–2498.
[7] K.H. An, W.S. Kim, Y.S. Park, Y.C. Choi, S.M. Lee, D.C. Chung, D.J. Bae, S.C. Lim, Y.H. Lee, Adv. Mater. 13 (2001) 497–500.
[8] A. Burke, J. Power Sources 91 (2000) 37–50.
[9] P. Simon, Y. Gogotsi, Nat. Mater. 7 (2008) 845–854.
[10] J.R. Miller, P. Simon, Science 321 (2008) 651–652.
[11] F. Lufrano, P. Staiti, Electrochim. Acta 49 (2004) 2683–2689.
[12] E. Frackowiak, Phys. Chem. Chem. Phys. 9 (2007) 1774–1785.
[13] J. Huang, B.G. Sumpter, V. Meunier, Angew. Chem. Int. Ed. 47 (2008) 520–524.
[14] T. Brezesinski, J. Wang, S.H. Tolbert, B. Dunn, Nat. Mater. 9 (2010) 146–151.
[15] M. Toupin, T. Brousse, D. Bélanger, Chem. Mater. 16 (2004) 3184–3190.
[16] B.E. Conway, V. Birss, J. Wojtowicz, J. Power Sources 66 (1997) 1–14.
[17] H. Zhang, X. Yu, P.V. Braun, Nat. Nano 6 (2011) 277–281.
[18] C. Meng, C. Liu, L. Chen, C. Hu, S. Fan, Nano Lett. 10 (2010) 4025–4031.
[19] Y. Ding, M. Chen, MRS Bull. 34 (2009) 569–576.
[20] L.Y. Chen, T. Fujita, Y. Ding, M.W. Chen, Adv. Funct. Mater. 20 (2010) 2279–2285.
[21] L. Nyholm, G. Nyström, A. Mihranyan, M. Strømme, Adv. Mater. 23 (2011) 3751–3769.
[22] P. Novák, K. Müller, K.S.V. Santhanam, O. Haas, Chem. Rev. 97 (1997) 207–282.
[23] H.E. Katz, P.C. Searson, T.O. Poehler, J. Mater. Res. 25 (2010) 1561–1574.
[24] G.A. Snook, P. Kao, A.S. Best, J. Power Sources 196 (2011) 1–12.
[25] P.G. Bruce, B. Scrosati, J.-M. Tarascon, Angew. Chem. Int. Ed. 47 (2008) 2930–2946.
[26] X. Lang, A. Hirata, T. Fujita, M. Chen, Nat. Nano 6 (2011) 232–236.
[27] X. Lang, L. Zhang, T. Fujita, Y. Ding, M. Chen, J. Power Sources 197 (2012) 325–329.
[28] F. Meng, Y. Ding, Adv. Mater. 23 (2011) 4098–4102.
[29] H.-J. Jin, S. Parida, D. Kramer, J. Weissmüller, Surf. Sci. 602 (2008) 3588–3594.
[30] J. Erlebacher, M.J. Aziz, A. Karma, N. Dimitrov, K. Sieradzki, Nature 410 (2001) 450–453.
[31] X.Y. Lang, L.Y. Chen, P.F. Guan, T. Fujita, M.W. Chen, Appl. Phys. Lett. 94 (2009) 213109.
[32] X.Y. Lang, H.T. Yuan, Y. Iwasa, M.W. Chen, Scripta Mater. 64 (2011) 923–926.
[33] Q. Wu, Y. Xu, Z. Yao, A. Liu, G. Shi, ACS Nano 4 (2010) 1963–1970.
[34] J. Wang, Y. Xu, J. Zhu, P. Ren, J. Power Sources 208 (2012) 138–143.
[35] Y. Furukawa, S. Tazawa, Y. Fujii, I. Harada, Synth. Met 24 (1988) 329–341.